Chemical Bulletin of "Politehnica" University of Timisoara, ROMANIA
Series of Chemistry and Environmental Engineering
Chem. Bull. "POLITEHNICA" Univ. (Timisoara) ***Volume 60(74), 2, 2015***

Corrosion Behavior of WC-Ni Coatings Deposited by Different Thermal Spraying Methods

I. Hulka[*], D. UTu[*], V.A. Serban[*], M.L. Dan[*], V. Matikainen[*] and P. Vuoristo[*]

[*] Politehnica University of Timisoara, P-ta Victoriei, Nr 2, 300006, Timisoara, Romania
email: iosif.hulka@upt.ro

[**] Tampere University of Technology, Department of Materials Science, FI-33720, Finland

Abstract: This study compares the properties of WC-Ni coatings manufactured from fine powder particles using high-velocity oxygen fuel (HVOF) and high-velocity air fuel (HVAF) spraying processes. The results indicated that the decarburization of carbide phase is influenced by the spraying equipment. It was found out that the deposition velocity is an important factor influencing the bonding between splats and furthermore the coating density. The WC-Ni coating sprayed with the supersonic M3 HVAF spraying gun revealed the lowest degree of porosity and degree of decarburization, achieving the best properties in terms of electrochemical corrosion resistance when compared to the HVOF sprayed WC-Ni coating.

Keywords: WC-Ni, hard coatings, cermet, corrosion studies, thermal spraying

1. Introduction

Thermal spraying is a deposition technique in which molten, semi-molten or solid particles are deposited on a certain surface [1]. The coating is formed by continuous impacts of accelerated droplets on the substrate. At impact the particles deform into thin lamellar shapes (splats), overlap and interlock as they solidify and cool down [2]. A device called spray gun is used to accelerate the heated particles. The feedstock material can be in the form of stick, wire or powder which is fed into the flame produced by the spraying gun. The high temperature and kinetic energy of the particles is obtained by burning mixtures of different fuel gases or kerosene with oxygen, or by using electrical power sources.

The high-velocity oxygen fuel (HVOF) spray processes uses thermal and kinetic energy to melt the feedstock powder and to accelerate the particles towards the surface, respectively. In HVOF spraying the fuel is burnt with oxygen at a high pressure generating a high velocity jet. For HVOF spraying the typical fuels are gases such as propane, ethylene, propylene, hydrogen and methylacetylene-propadiene-propane (MAPP) mixture or liquid kerosene. Usually the temperature varies between 2500 °C and 3200 °C depending on the fuels [3] which generate particle velocities up to 750 m/s [4]. High-velocity air fuel (HVAF) spray process is a similar but more economical method compared to HVOF spraying [5]. High velocity air-fuel (HVAF) thermal spraying is a newer developed spraying process for deposition of metallic and carbide based coatings from powder feedstock [6]. During the spraying process the powder particles are heated below their melting point (under 2000°C) and accelerated to velocities above 700 m/s which makes the process a solid spraying technology in which spraying temperature is an important parameter for coating deposition [5, 7]. The new M3 supersonic spray gun represents the state of the art in HVAF spraying. It can produce high particle velocities up to 1200 m/s and high particle temperatures compared to single nozzle HVAF spraying guns which allows producing dense and hard coatings [7].

The objective of this study is to investigate the influence of deposition method on the microstructure and corrosion properties of the HVOF and HVAF sprayed coatings.

2. Experimental

The WC-Ni coatings were deposited onto low carbon steel substrates by HVOF and HVAF spraying techniques using a commercial WC-Ni (Ni ~ 10%, C ~5.4%, W - balance) powder manufactured by Buffalo Tungsten Inc., US, as the feedstock material. Angular alumina was used as an abrasive media for substrate preparation in order to increase the surface roughness before spraying. The HVAF spraying was carried out using a Supersonic Air Fuel HVAF (SAF) M3 (Uniquecoat Technologies LLC, US) spray gun while the HVOF spraying was carried out with a DJ 2700 (Sulzer Metco, US) spraying gun. The coating cross-sections were examined using a Quanta FEG 250 (FEI, The Netherlands) scanning electron microscope (SEM) equipped with EDAX analyzer. The porosity within the coatings was determined by image analysis using image processing software, Image Tool 3.00, onto 12 backscattered electron micrographs at 2000X magnification. Micro-hardness was measured with a Matsuzawa MMT X7 tester using 300g load for 10 indentations per sample. X-ray diffractometry (XRD) of powder and as-sprayed coatings was performed on an Empyrean diffractometer (PANAnalytical, The Netherlands) using Cu-Kα radiation. The measurements were performed at 2θ diffraction angle in the range of

20°–100° and with 0.02° step size. Phase identification was performed using the PANAnalytical X'Pert High Score Plus software using the ICDD JCPDF-2 database (International Centre for Diffraction Data, Newtown Square, US).

Electrochemical tests were performed at room temperature using a SP-150 potentiostat/galvanostat (Bio-Logic, SAS, France) using a typical glass cell equipped with three electrodes: working electrodes consisting of WC-Ni coated samples deposited by HVOF and HVAF spraying processes, Ag/AgCl reference electrode and a platinum mesh used as counter electrode. For the experiments the exposed surface of specimens was 1 cm^2, submerged in a 3.5 wt. % NaCl solution. The electrode potential was stabilized for 60 min to achieve the equilibrium.

3. Results and Discussion

3.1. Powder characterization

Figure 1a shows a representative image of the WC-Ni powder particles used in the present study. The powder was manufactured by agglomeration and sintering process. The size distribution of the particle granules was in the range of 7-21 µm and the powder morphology consisted of spherical and irregular particles. For thermal spraying the preferable shape of the powder particles is spherical in order to increase the flowability during deposition. The irregular shape and small size of the particles can lead to poor powder feeding during the spraying process which can have a strong influence on the coatings properties. The EDX spectrum of the powder is presented in Figure 1b and confirms the powder chemical composition, the identified elements being carbon, tungsten and nickel.

3.2. Coating microstructure

Metallographic images of cross-sectional microstructure of the two sprayed coatings are presented in Figure 2. Both coatings are dense and a good adhesion to the substrate can be noticed. Some cracks can be observed in the upper region of the HVOF coating which might be attributed to the rapid cooling and solidification process. In comparison, the HVAF coating looks denser and free of major defects but due to the very fine powder and the presence of irregular shape powder particles the flowability during deposition was affected and the deposition efficiency was lower which conducted to a thinner coating.

Using the HVOF thermal spraying method a thicker coating was obtained with a thickness of about 260 micrometers compared to the HVAF deposited coating with a thickness of 100 micrometers.

The micro-hardness determined on the cross section of the coatings showed different results regarding the recorded values. The coatings produced by HVAF thermal spraying had higher hardness values than the HVOF sprayed coatings, as listed in Table 1, which might be attributed to hard phases formed during spraying due to higher intralamellar hardness [8]. The porosity of the coatings was analyzed from the metallographic images with the corresponding software and the results were 1.85% for the HVOF coating and 0.23% for the HVAF coating, as listed in Table 1. This indicates that the HVAF coating had a denser structure due to the M3 gun which produces higher particle velocities compared to the DJ 2700 gun.

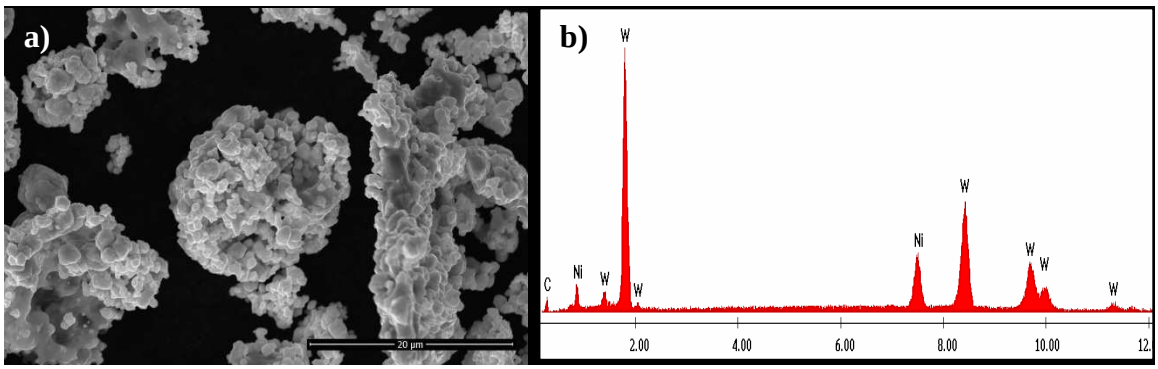

Figure 1. Morphology (a) and EDX spectra (b) of WC-Ni powder

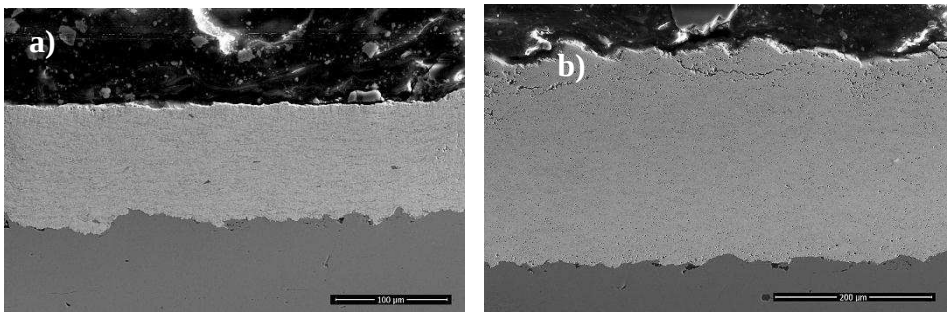

Figure 2. SEM micrographs of HVOF (a) and HVAF (b) WC-Ni coatings in cross-sections

TABLE 1. Thickness, hardness and porosity of thermally sprayed WC-Ni coatings

Material	Coating thickness [µm]	Micro-hardness HV0.3	Porosity [%]
WC-Ni HVOF	262.16 ± 18.92	747 ± 115	1.85
WC-Ni HVAF	99.02 ± 21.2	1395 ± 47	0.23

The XRD patterns of the used WC-Ni powder and the two sprayed coatings are presented and compared in Figure 3. The analysis of the XRD patterns confirms that the powder consists of WC phase and metallic γ-Ni phase. The spectrum for the coatings predominantly consists of WC phase while also W_2C can be detected. The intensity of the W_2C peaks is lower for the HVAF sprayed coating indicating lower degree of decarburization. The M_xC peaks might correspond to phase dissolution of the carbide phase in the molten Ni matrix. It is thought that a reduction in flame temperature during thermal spraying led to a decrease of decomposition of WC phase which means that no significant transformation took place during deposition.

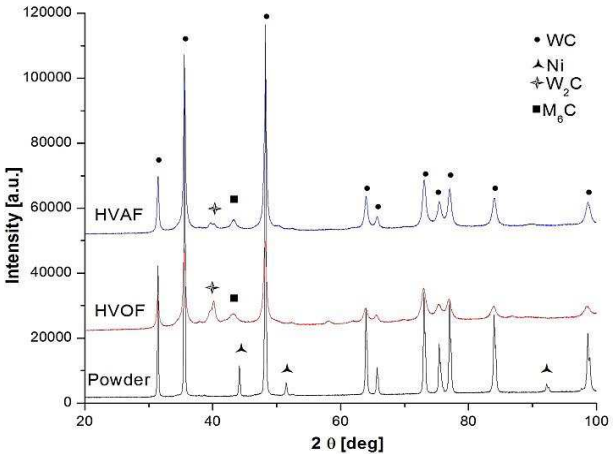

Figure 3. X-ray diffraction (XRD) patterns of investigated WC-Ni powder and deposited HVOF and HVAF coatings

3.3. Corrosion behavior

3.3.1. Open circuit potential

The evolution in time of the equilibrium potential of the tested samples (electrodes) is twofold: first, it allows an assessment of the corrosion behavior of the exposed surface to the corrosive media, and secondly allows the estimated time to reach a stationary or quasi-stationary state. In Figure 4, open cell potentials of the two sprayed coatings are compared. At the beginning of the test the coatings present an unstable open cell potential indicating corrosion activity afterwards the potentials started to stabilize. According to the obtained chart, it can be noticed that after 1 hour of testing, the system had reached a quasi-stationary state, enough to start the linear polarization measurements.

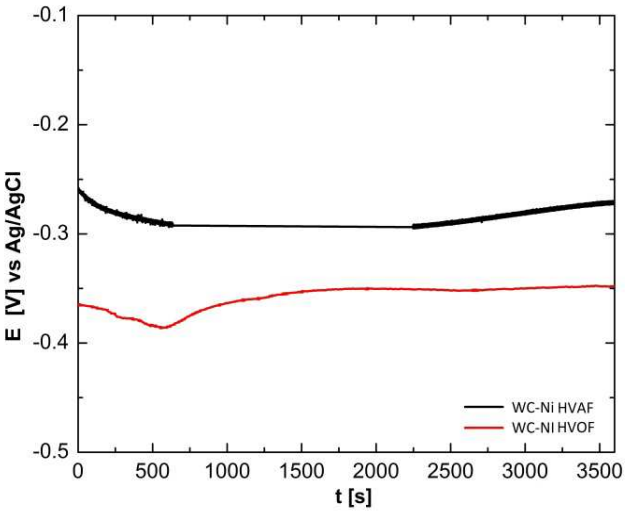

Figure 4. Open circuit potential (E_{OCP}) measurements of WC-Ni coatings

Within the WC coating, the open circuit potential of the carbide phase is much nobler than that of the metallic matrix and substrate. The open circuit potential difference between WC and Ni causes micro-galvanic corrosion when the electrolyte is in contact with the surface of the coating. In that case the WC phase becomes cathodic and Ni becomes anodic, resulting in corrosion of anodic binder material. Also, when the electrolyte infiltrates along the micro-cracks and pores existing in the coating, the macro-galvanic corrosion can occur [9].

The values obtained after measurements reaching the quasi-stationary state are shown in Table 2. The presented data confirms that the electrode movement towards a more positive value leads to a decrease in the speed of polarization which means better corrosion behavior. The HVAF coating indicated better corrosion behavior due to lower porosity which might be attributed to a denser coating deposited at higher velocities.

TABLE 2. E_{OCP} at 25˚C

Electrolyte	Sample	Temperature [˚C]	E_{OCP} [V]/Ag/AgCl
NaCl 3,5%	WC-Ni HVOF	25˚C	-0,271
	WC-Ni HVAF		-0,344

3.3.2 Potentiodynamic polarization studies

This method enables immediate corrosion rate determination via the intensity of the corrosion current and Tafel slopes but also shows possible changes at the electrode surface or changes in the mechanism of corrosion process. In the present study, a sweep potential of ±250 mV was applied against the open cell potential and a scan speed of 1 mVs^{-1} was used. By this method the corrosion rate can be calculated using the direct substitution of Tafel slope values (cathodic - b_c and anodic - b_a) using the following equation:

$$i = i_{cor}\left\{exp\left[\frac{2,303}{b_a}(E - E_{cor})\right] - exp\left[-\frac{2,303}{b_c}(E - E_{cor})\right]\right\} \quad (1)$$

were $\frac{2,303}{b_a}$ represents the anodic slope and $\frac{2,303}{b_c}$ respectively the cathodic slope; Tafel slope constants associated with anodic (b_a) and cathodic (b_c) processes; E and E_{cor} - potential and corrosion potential ; i_{cor} - corrosion current density. Linear polarization curves recorded for WC-Ni coatings in 3.5% NaCl at 25°C are presented in Figure 5.

In order to determine the electrochemical parameters the polarization curves were fitted and the results are presented in Table 3. The HVAF coating exhibits better corrosion resistance indicated by the lower passive current density and wide passive region due to a denser coating, reduced porosity and micro-cracks compared to the HVOF coating.

3.3.3 Electrochemical Impedance Spectroscopy

This method represents a stationary electrochemical technique based on overlapping a low amplitude alternative signal (which contains an excitation frequency) above the electrode potential and tracking the electrode response at this perturbation. While the electrochemical system behaves like a nonlinear system its impedance will be dependent on the potential. Analyzing the response provided by the system the interface structure can be determined and also the reactions which take place at the coating/electrolyte interface by proposing and equivalent electric circuit for process simulation. In the case of corrosion, the polarization resistance of working electrode depends on the micro-cracks and porosity within the coating. The obtained results by carrying out this type of measurement are expressed by so called Nyquist and Bode diagrams [10, 11] presented in Figure 6.

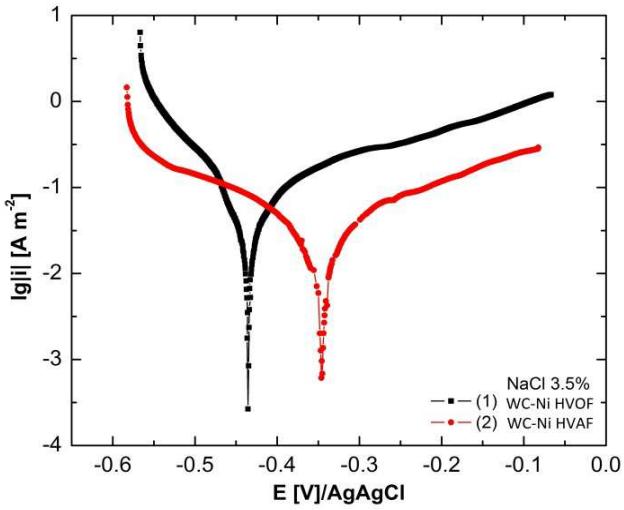

Figure 5. Polarization curves of WC-Ni coatings

The Nyquist plot for the HVAF coating shows the presence of an incomplete semicircle attributed to a depressed capacitive loop at high to intermediate frequency range [12]. Deviation of recorded circle from the perfect circular shape can be associated with electrode superficial inhomogeneity, which might be noticed for the HVOF coating. This superficial inhomogeneity, is caused as effect of surface roughness or different interfacial phenomena. These spectra were fitted using the equivalent circuit shown in Figure 7 in order to determine the experimental values presented in Table 4.

When analyzing the equivalent circuit presented in Figure 7 it can be observed that the system consists of four components: R_s – solution resistance, *CPE* – constant phase element which represent a modified capacitance that is a frequency dependent element and is related to the surface roughness [14], R_{ct} – charge transfer resistance and W – Warburg impedance which is associated with mass transport process. Presence of Warburg impedance suggested that the corrosion reaction is limited by mass transport. Based on presented circuit were obtained the parameters associated with corrosion process. Electrical circuit used for modeling of experimental EIS data consist of a serial connection between solution resistance R_s and a parallel connection of the constant phase connection *CPE* and the charge transfer resistance R_{ct} in series with a Warburg impedance.

TABLE 3. Electrochemical parameters obtained from polarization curves

TS	*M echiv.* [g]	*Dens.* [g cm^{-3}]	i_{cor} [μA cm^{-2}]	E_{cor} [mV]	$-b_c$ [mV dec^{-1}]	b_a [mV dec^{-1}]	R_p [Ω]	v_{cor} [mm an^{-1}]
HVOF	38.56	4.0	6.21	-435	96	208	3017	0.20
HVAF	38.56	4.0	3.57	-346	256	281	7514	0.11

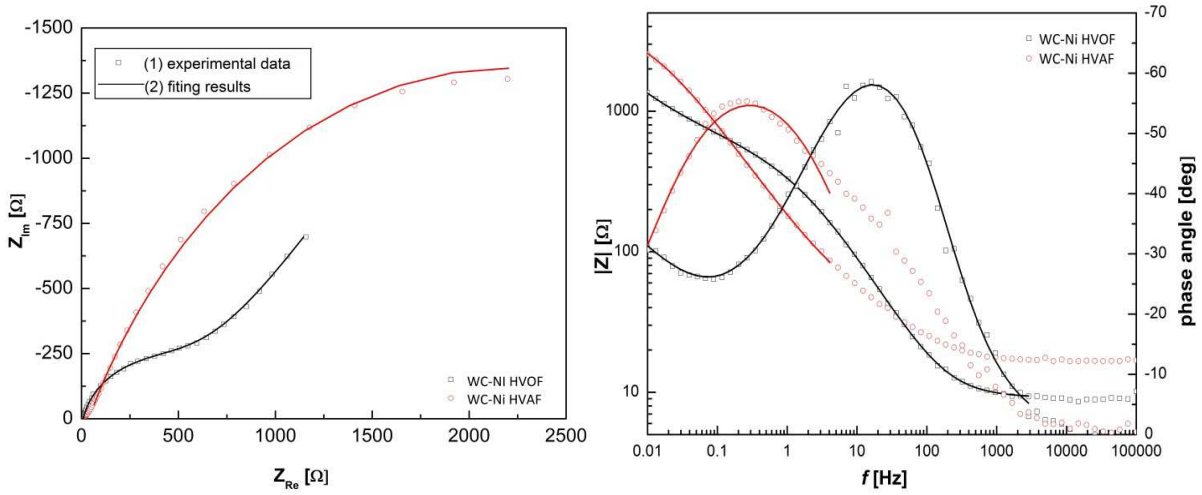

Figure 6. Nyquist (a) and Bode (b) plots obtained in NaCl 3,5% solution at 25°C for WC-Ni coatings

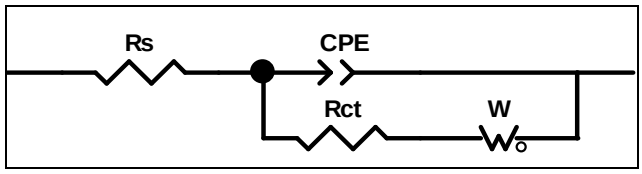

Figure 7. Equivalent circuit for spectra fitting

TABLE 4. Experimental values of EIS during the corrosion process

TS	R_s [Ω cm^2]	T [F cm^{-2} s^{n-1}]	n	R_{ct} [Ω cm^2]	C_{dl} [μF cm^{-2}]	Chi^2
HVOF	9,14 (0,7%)	3,2 10^{-4} (3,16%)	0,83 (0,62%)	182,4 (1,32%)	114	7,3 10^{-4}
HVAF	36,9 (1,43%)	1,63 10^{4} (0,61%)	0.71 (0,61%)	433 (2,62 %)	516	8,8 10^{-4}

Impedance of constant phase element is described by:

$$Z_{CPE} = 1/T(j\ \omega)^n \quad (2)$$

where 0 < n <1 and is describing the constant phase angle of CPE, Y0 is a parameter related to the double layer capacitance [6].

Impedance of Warburg element in case of a finite length thickness of diffusion layer δ can be expressed:

$$Z_w = (R_w(j\ \omega\tau_D)^{-\phi}) \tan (j\ \omega\tau_D)^{\phi} \quad (3)$$

where R_w – diffusion resistance; τD – diffusion time constant given by $\tau_D = \delta^2/D$, where δ – diffusion thickness and D – diffusion coefficient; φ – an exponent whit values between 0 and 1 [14].

After modeling of experimental data using CNLS procedure for both superficial layers are presented in Table 4. The charge transfer resistance is associated with the occurrence of the charge transfer reaction at the bottom of pores present in the coating layer. In the case of HVAF coating the R_{ct} is more than two times higher in comparison with HVOF coating. The higher value can be attributed to the effective barrier behavior. EIS measurements therefore show that the HVAF coating possesses less interconnected porosity and micro-cracks which indicate through electrochemical characteristics that the coating is nobler than HVOF coating.

4. Conclusions

In the present study the properties of WC-Ni coatings manufactured by DJ 2700 HVOF gun and M3 HVAF torch were assessed and compared. The experimental results lead to the following conclusions:

- Hard and dense WC-Ni coatings can be obtained by using the HVOF and HVAF processes to spray fine feedstock powder. The coatings sprayed by HVAF method are denser and exhibit less pores and cracks.

- WC dissolution is reduced in the metallic matrix and no significant decarburization took place during the coating deposition with HVAF spraying.

- Due to the supersonic speed of HVAF spraying the powder particles are projected with higher velocity leading to denser coatings with reduced porosity (<0.5%) and less cracks within the coatings. This has a positive effect on the corrosion behavior of the coating compared to HVOF manufactured coating.

- The thickest coating (260 µm) deposited by HVOF spraying is less protective than the thinner HVAF sprayed coating (100 µm) in 3.5% NaCl solution.

ACKNOWLEDGEMENT

This work was supported by the strategic grant POSDRU/159/1.5/S/137070 (2014) of the Ministry of National Education, Romania, co-financed by the European Social Found – Investing in people, with the Sectorial Operational Program Human Resources Development 2007-2013.

REFERENCES

1. Pawlowski L., The science and engineering of thermal spray coatings, Ed. John Wiley and Sons, **2008**.
2. Schneider K.E., Belashchenko V., Dratwinski M., Siegmann S. and Zagorski A., Thermal spraying for Power Generation Components, WILEY-VCH Verlag GmbH & Co. KGaA, Weinheim, **2006**.
3. Turunen E., Diagnostic tools for HVOF process optimization, Dissertation for the degree of Doctor of Science in Technology, VTT Industrial Systems, Helsinki, **2005**.
4. Davis J R., Handbook of Thermal Spray Technology, ASM International, **2004**.
5. Zhou X.I. and Zhang J.S., *Transaction of Nonferrous Metals Society of China*, 18, **2008**, 262-269.
6. Verstak A. and Baranovski V., Thermal Solution: Advances in Technology and Applications, 10-14 May, Osaka, DVS: German welding society, **2004**, 551-555.
7. Uniquecoat Technologies Inc. website: www.uniquecoat.com
8. Verdom C., Karimi A. and Martin J.L., *Materials Science and Engineering A*, 246, **1998**, 11-24.
9. Cho J. E., Hwang S.Y. and Kim K.Y., *Surface and Coatings technology*, 200, **2006**, 2653-2662.
10. Orazem M.E. and Trobollet B., Electrochemical impedance spectroscopy, Ed. Wiley, **2008**.
11. Barsoukov E. and Macdonald J. R., Impedance spectroscopy theory, Experiment and Applications, Ed. Wiley Interscience, **2005**.
12. Ashassi-Sorkhabi H., Ghalebsaz-Jeddi N., Hashemzadeh F. and Jahani H., *Electrochimica Acta*, 51, **2006**, 3848-3854.
13. Lecante A., Robert F., Blandinieres P.A. and Roos C., *Current Applied Physics*, 11, **2011**, 714-724.
14. Kellenberger A. and Vaszilcsin N., Micro si Nanomateriale, Electrochimia starii solide, Ed. Politehnica, **2013**.

Received: 12 October 2015
Accepted: 24 November 2015

.